



## OPEN ACCESS

## EDITED BY

Xia Wang,  
Chengdu University of Technology, China

## REVIEWED BY

Long Luo,  
Chongqing University of Science and  
Technology, China  
Jie Li,  
China University of Geosciences Wuhan,  
China

## \*CORRESPONDENCE

Huoqing Gao

✉ gaohuoqing0229@outlook.com

RECEIVED 07 April 2025

ACCEPTED 27 May 2025

PUBLISHED 17 June 2025

## CITATION

Wang G, Gao H and Zou H (2025) Sequence stratigraphy and geometry of the carbonate platform in the Longwangmiao Formation (Toyonian), Cambrian, SW China. *Front. Mar. Sci.* 12:1607571. doi: 10.3389/fmars.2025.1607571

## COPYRIGHT

© 2025 Wang, Gao and Zou. This is an open-access article distributed under the terms of the [Creative Commons Attribution License \(CC BY\)](https://creativecommons.org/licenses/by/4.0/). The use, distribution or reproduction in other forums is permitted, provided the original author(s) and the copyright owner(s) are credited and that the original publication in this journal is cited, in accordance with accepted academic practice. No use, distribution or reproduction is permitted which does not comply with these terms.

# Sequence stratigraphy and geometry of the carbonate platform in the Longwangmiao Formation (Toyonian), Cambrian, SW China

Guangwei Wang<sup>1,2</sup>, Huoqing Gao<sup>1,2\*</sup> and Huayao Zou<sup>3,4</sup>

<sup>1</sup>State Key Laboratory of Deep Oil and Gas, China University of Petroleum (East China), Qingdao, Shandong, China, <sup>2</sup>School of Geoscience, China University of Petroleum (East China), Qingdao, Shandong, China, <sup>3</sup>State Key Laboratory of Petroleum Resources and Prospecting, China University of Petroleum (Beijing), Beijing, China, <sup>4</sup>College of Geosciences, China University of Petroleum (Beijing), Beijing, China

Carbonate platforms provide important sedimentary archives for paleoceanography and recording paleoenvironments. The aim of this study was to decipher the control of platform evolution and its constraint on the chemostratigraphic correlation in the Lower Cambrian at the eastern part of the Yangtze Platform. With the petrological observation, XRD, as well as C and O isotope analysis, two third-order sequences (SQ1 and SQ2) and six fourth-order sequences (PSQ1, PSQ2, PSQ3, PSQ4, PSQ5, and PSQ6) were recognized in the Longwangmiao Formation. Thirteen lithofacies (Lf-1–Lf-13) and three facies associations (shoreface, upper offshore, and lower offshore) were identified across the proximal to distal range of the platform. The correlation between logged outcrop sections suggested that the carbonate platform evolved from a homoclinal ramp in PSQ1 to a more distally deepened geometry in PSQ2, with this evolution driven by synsedimentary fault activity. From PSQ2 to PSQ3, the geometry evolved from a ramp to a rimmed platform associated with depleted  $\delta^{13}\text{C}$  values and an increasing Chemical Index of Alteration (CIA) index. Such a transition of platform geometry may be attributed to the enhanced rate of carbonate production due to intense weathering and nutrient input. The final evolution of the Eastern Yangtze Platform (PSQ4) seemed to have been driven by falling relative sea levels and resulted in the formation of a flat-topped morphology, associated with subaerial exposure and depleted  $\delta^{13}\text{C}$  (LNE2). The two final sequences recognized in outcrops, PSQ5 and PSQ6, were only recognized in the distal reaches of the deposit and were interpreted to be “missed beats” in the sense that the sea level did not transgress the platform top. This study suggests the importance of carbonate production driven by chemical weathering on the control of platform geometry and sequence stratigraphy.

## KEYWORDS

sequence stratigraphy, platform geometry, carbonate production, chemical weathering, Longwangmiao Formation, South China

## 1 Introduction

Carbonate platforms, as a main component of marine depositional systems, are fundamentally shaped by eustatic sea level fluctuations, carbonate production, and tectonic subsidence. The interaction of those factors can lead to a change in the types of carbonate platforms (ramp and rimmed platforms) (Read, 1985; Schröder et al., 2005; Tucker and Wright, 1990; Vail et al., 1977), and the resultant depositional records can reflect paleoceanographic chemistry, biotic communities, tectonic activity, and paleoclimatic perturbations (Chen et al., 2024; Kelley et al., 2017; Li et al., 2012). The Cambrian Period, marking the onset of widespread Phanerozoic carbonate platform development, witnessed platform evolution closely linked with global transgressive events, the Cambrian Explosion, and tectonic activities (Pfeil and Read, 1980; Saltzman, 1999). However, the impact of abundant terrigenous detritus derived from active tectonic settings on adjacent carbonate depositional systems remains a significant subject (Hallock and Schlager, 1986; Jin et al., 2018; Lokier et al., 2009; Mutti and Hallock, 2003). On the one hand, terrigenous influx may suppress platform development through multiple mechanisms: it can elevate nutrient concentrations that degrade water quality and reduce light penetration, thereby inhibiting the growth of carbonate-producing organisms (Hallock and Schlager, 1986; Mutti and Hallock, 2003), or directly cover the carbonate basement, limiting benthic attachment and carbonate precipitation as well as changing the concentration of water chemistry to inhibit the precipitation of carbonates (Kumpan et al., 2019; Lokier et al., 2009; Šimiček et al., 2020; Woolfe and Larcombe, 1999). On the other hand, moderate terrigenous input may sustain or even enhance platform accretion. Clay-grade particulates exhibit negligible interference with coral growth (Lokier et al., 2009), while coarser clastic grains (e.g., quartz and feldspar) can serve as cores for ooid development, facilitating carbonate shell formation. Notably, ooids demonstrate remarkable resilience to terrigenous influx, with documented occurrences even within dominantly terrigenous detritus depositional systems (Loreau and Purser, 1973). Therefore, it is still a challenge to decipher the control of carbonate production induced by chemical weathering on the evolution of carbonate platforms.

The large-scale carbonate sediments occur in the Longwangmiao Formation of the Lower Cambrian and thus offer an opportunity to decipher the geometry of carbonate platforms. Regarding the type of carbonate platform, previous studies have suggested that the Upper Yangtze Platform was in its initial growth stage and lacked reef builders, resulting in the formation of a characteristic carbonate ramp (Du et al., 2016; Jin et al., 2025; Liu et al., 2018; Mei et al., 2006; Zhang et al., 2019). In contrast, a rimmed platform was induced by a wide restricted platform with a visible platform margin and slope (Shen et al., 2018; Xie et al., 2024). Therefore, further research on the depositional model of the Cambrian Longwangmiao Formation in the Sichuan Basin, as well as the impact of terrestrial detritus on carbonate production, is necessary. Overall, the aims of this study were 1) to reconstruct the sequence stratigraphic framework of the Yangtze Platform, 2) to

analyze the evolution from a ramp to a rimmed platform, and 3) to evaluate the influence of terrigenous detritus on carbonate production.

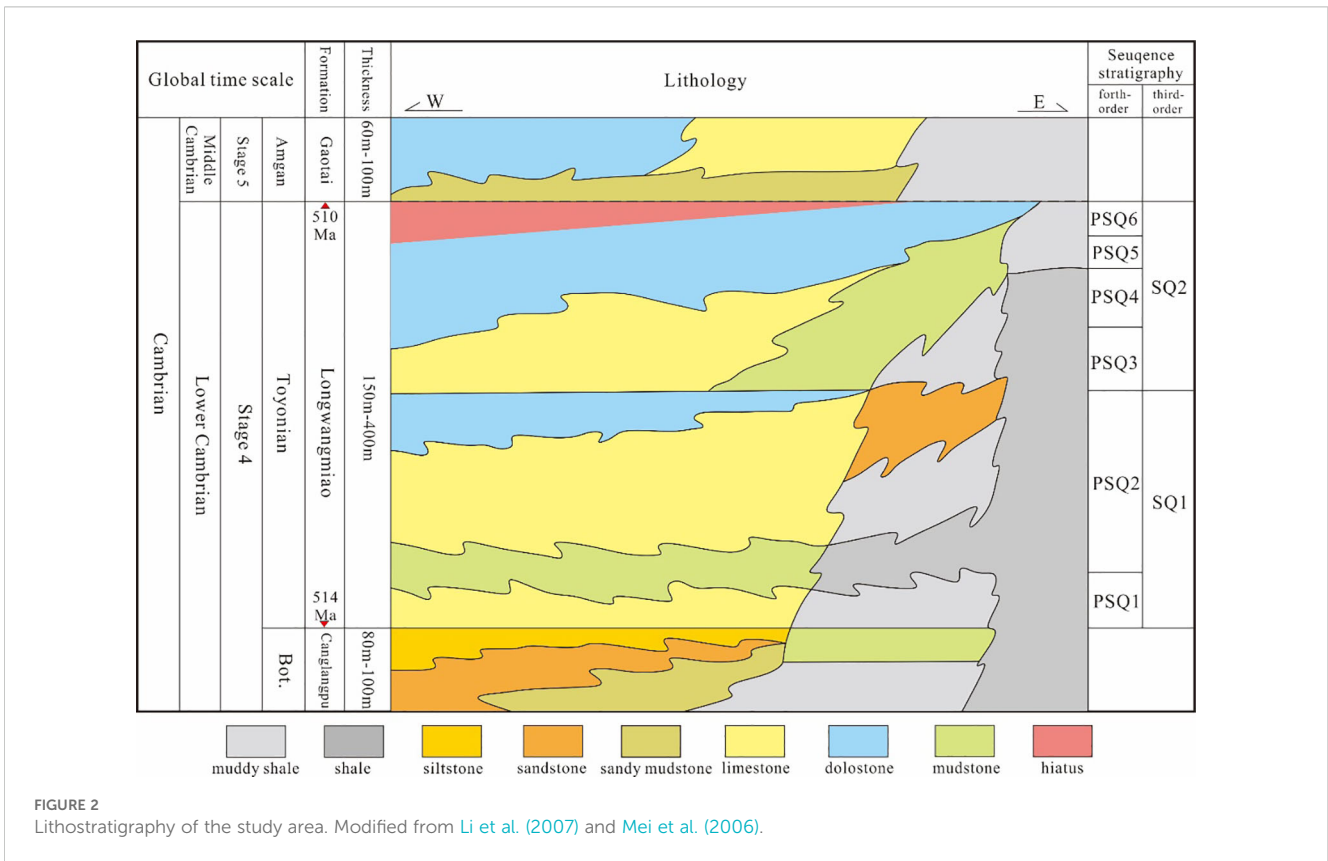
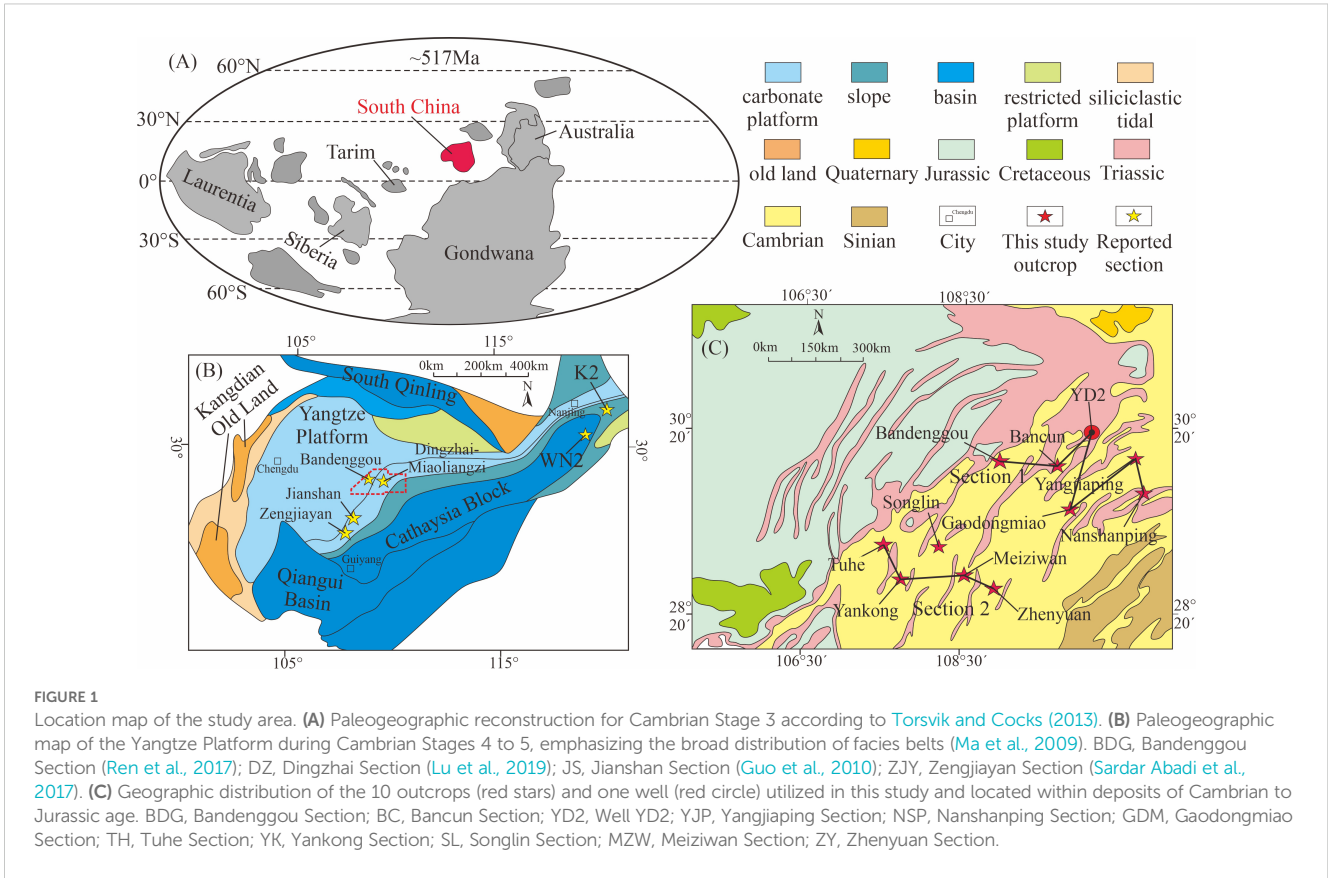
## 2 Geological setting

In the Early Cambrian, South China was an isolated craton located at approximately 20°N paleolatitude and situated to the north of Gondwana (Figure 1A). During the Longwangmiao Period, the Yangtze Platform dominated the craton, was situated in an extensional setting, and comprised thick carbonate sequences (Huang et al., 2011). Currently, the southern margin of the Yangtze Platform is adjacent to the Cathaysia Block, and the platform's western margin abuts the Kangdian Old Land. The South Qinling, meanwhile, lies to the north of the platform (Zhou et al., 2014). As portrayed in Figure 1B, four broad facies belts developed on top of the craton, and each is associated with a different depositional environment. The first facies belt is dominated by carbonate sediments, and the second, which is restricted to the west of the Yangtze Platform, is rich in siliciclastics and associated with the Kangdian Old Land. The third belt comprises a slope facies that lies outboard of the northern and southern platform margins. Finally, the fourth facies belt was interpreted to be basinal in origin and best represented in the east to southeast of the platform. The study area considered in this paper extends over 70,000 km<sup>2</sup> of the southeastern reaches of the Yangtze Platform.

The Longwangmiao Fm. (510–514 Ma), which corresponds to the Toyonian in Cambrian Stage 4, underlies the Gaotai Fm. and overlies the Canglangpu Fm. (Figure 2). The upper boundary of the Longwangmiao Fm., separating the Early Cambrian from the Middle Cambrian, occurs in the shallow-water deposits to the west of the study area where it is manifested as a regressive–transgressive sequence marked by a hiatus in the deposition of shallow-water carbonates. The transition between the Longwangmiao Fm. and the underlying Canglangpu Fm. is marked by a change from terrestrially derived siliciclastics to shallow-marine carbonate sediments, indicative of a transgressive surface (Mei et al., 2006; Ma et al., 2009). The Longwangmiao Fm. is divided into a pair of third-order sequences (SQ1–SQ2) and five fourth-order sequences (PSQ1–PSQ6). It should be noted, however, that PSQ5 and PSQ6 were only recognized in the deeper water setting to the east of the study area, as it is hiatal on the platform top, which lies to the west.

## 3 Methods

In order to characterize the sedimentology, 10 outcrops and one core were logged (locations shown in Figure 1C). A total of 320 thin sections were cut from samples collected in the field and representing all aspects of the considered stratigraphy. Dominant rock texture was determined for each section using a polarizing microscope and following the classification scheme of Embry and Klovan (1971). Petrographic thin sections were observed using a



Leica DM-4500 microscope, and cathodoluminescence analyses were performed using a RELIOTRON III (with an operating current of 10–12 kV) of the China University of Petroleum (Beijing, China).

A total of 180 samples of the sections and cores were collected. All samples were milled to powder (~200 mesh) using an agate mortar and prepared for stable carbon and oxygen analysis. Prior to testing, the Mn and Sr contents of the samples from previous studies (Lu et al., 2025) were determined, and Mn/Sr values were calculated to exclude the effect of diagenetic alterations.  $\delta^{13}\text{C}$  and  $\delta^{18}\text{O}$  data were obtained using a Finnigan MAT 253 mass spectrometer.  $\text{CO}_2$  extracted from each powdered sample was digested by anhydrous phosphoric acid (100%) in sealed tubes on an auto sample-handling machine for 2 hours. An acid fractionation factor of 1.01024 (Friedman and O'Neil, 1977) for calcites was utilized to calculate isotopic values. All  $\delta^{13}\text{C}$  and  $\delta^{18}\text{O}$  values were reported in per mil (‰) relative to Vienna Pee Dee Belemnite (VPDB). The standard samples were from Chinese national standards of GBW04416 ( $\delta^{13}\text{C} = +1.61\text{‰} \pm 0.03\text{‰}$ ,  $\delta^{18}\text{O} = -11.59\text{‰} \pm 0.11\text{‰}$ ) and GBW04417 ( $\delta^{13}\text{C} = -6.06\text{‰} \pm 0.06\text{‰}$ ,  $\delta^{18}\text{O} = -24.12\text{‰} \pm 0.19\text{‰}$ ), as well as the international standards of NBS-18 ( $\delta^{13}\text{C} = -5.01\text{‰} \pm 0.06\text{‰}$ ,  $\delta^{18}\text{O} = -23.00\text{‰} \pm 0.1\text{‰}$ ) and NBS-19 ( $\delta^{13}\text{C} = +1.95\text{‰}$ ,  $\delta^{18}\text{O} = -2.20\text{‰}$ ), to calibrate the experimental results. The precision and accuracy of the isotopic measurements were estimated to be higher than 0.1‰.

Twenty-nine rock samples, mainly collected from PSQ2 and PSQ3, were analyzed for major elements using an automatic X-ray fluorescence spectrometer at the Key Laboratory of Tectonics and Petroleum Resources at the China University of Geosciences (Wuhan). For details on this spectroscopy, see Wang and Zhou, (2000). The Chemical Index of Alteration (CIA) values obtained using this analysis have the potential to record the intensity of chemical weathering and associated climate conditions. The technique capitalizes on the fact that major-element geochemistry and siliciclastic mineralogy are strongly affected by chemical weathering (Nesbitt and Young, 1982; Yang et al., 2016). The CIA can be calculated using the molar proportions of each elemental species according to Equation 1 (McLennan, 1993):

$$\text{CIA} = \left[ \frac{\text{Al}_2\text{O}_3}{\text{Al}_2\text{O}_3 + \text{CaO}^* + \text{Na}_2\text{O} + \text{K}_2\text{O}} \right] \times 100 \quad (1)$$

where  $\text{CaO}^*$  represents only the CaO content in the silicate fraction. The samples were treated with HCl to dissolve the carbonate fraction of bulk samples. The residuals were dissolved in  $\text{HNO}_3$  to measure the major elements.

## 4 Results

### 4.1 Sedimentary facies

On the basis of examination of rock texture, grain type, fossils, and sedimentary structures, 13 lithofacies (Lf-1 through Lf-13) were identified and deemed to fall into three different depositional environments: 1) the shallowest depositional environment,

shoreface, lies above the fair-weather wave base and is encompassed by Lf-1 through Lf-5; 2) upper offshore, the second depositional environment, lies below the fair-weather wave base and above the storm wave base and contains Lf-6 through Lf-10; and 3) lower offshore is situated beneath the storm wave base and includes Lf-11 and Lf-13. The characteristics of the 13 lithofacies are as follows and summarized in Table 1.

#### 4.1.1 Shoreface lithofacies (Lf-1 through Lf-5)

Lf-1 is a massive gypseous mudstone characterized by a dolomitized micritic matrix with common fenestrate structures created by the dissolution of gypsum (Figure 3A). A proportion of these fenestral structures have been subsequently filled with microspar calcite cement (Figure 3B). The fenestrate structure and occurrence of the gypsum are consistent with deposition in a shallow hypersaline setting and possibly indicative of a tidal flat setting (Brigaud et al., 2009; Di Lucia et al., 2017). Within the sequence stratigraphic framework of the study area, Lf-1 was seen to develop during the rise and fall of sea level (Di Lucia et al., 2017).

Lf-2, a sandy mudstone, is a faintly laminated, well-sorted, and carbonate- to siliciclastic-rich (Figure 3C). This lithofacies, which is commonly associated with Lf-3 and Lf-4, coincides with transgressive episodes. Carbonate-rich intervals were deemed to be marine, whereas those dominated by siliciclastic grains were interpreted as having a terrigenous origin (likely associated with storm events, else riverine input, etc.; e.g., Andreucci et al., 2017; Sardar Abadi et al., 2017). The environment of deposition was assumed to be shallow-subtidal to lagoonal (Di Lucia et al., 2017; Sardar Abadi et al., 2017).

Lf-3 is composed of a medium- to well-sorted ooid grainstone displaying herringbone cross-bedding (Figure 3E), an indication of a high-energy shoal-water setting (Léonide et al., 2007). Bioturbation is rare, as is typical for such environments (Purkis et al., 2017). The ooids are coated with fibrous cement with local dissolution generating variable porosity (Figure 3D), likely induced by one or more episodes of subaerial exposure (Andreucci et al., 2017). Lf-3 is frequently found in association with Lf-2, Lf-4, and Lf-5. This lithofacies was interpreted to indicate early transgressive successions and complete regressive successions.

As depicted in Figures 3F, G, Lf-4 represents a peloidal packstone to grainstone with frequently developed cross-beds having thicknesses in the range of 10–20 cm, diagnostic features for a high-energy shoal or intertidal setting (Bover-Arnal et al., 2009; Elrick, 1996; Fallatah and Kerans, 2018). The units of this lithofacies are associated with Lf-2, Lf-3, and Lf-5.

The final lithofacies type associated with the shoreface depositional environment is Lf-5, a stromatolitic mudstone (Figure 3H), which was found in association with Lf-2, Lf-3, and Lf-4. The depositional setting was deemed to be shallow subtidal and medium- to low-energy (Elrick, 1996) (Elrick, 1996). Lf-5 was considered to be associated with regressive successions.

#### 4.1.2 Upper-offshore lithofacies (Lf-6 through Lf-10)

The first upper-offshore lithofacies, Lf-6, is a medium- to poorly sorted accumulation dominated by pisoids, ooids, and oncoids with

TABLE 1 Lithofacies descriptions and depositional environments developed in this study.

Lithofacies	Components	Depositional structures	Sorting and grain size	Inferred depositional environment
(Lf-1) Gypseous mudstone	Gypsum, micrite, peloids	Fenestral structure	<50 $\mu\text{m}$	Evaporitic supratidal and hypersaline, shoreface
(Lf-2) Sandy mudstone	Quartz, marls, micrite, peloids, mica, algae, echinoderm	Massive structure	Well-sorted, fine to medium rounding, <50 $\mu\text{m}$	Subtidal, lagoon, shoreface
(Lf-3) Ooid grainstone	Concentric ooids, peloids, spherulites, algae	Herringbone cross-bedding	Well-sorted and rounded, 200–1,000 $\mu\text{m}$	Shoal
(Lf-4) Peloidal grainstone/packstone	Peloids, ooids, spherulites, algae, brachiopods, mollusks	Planar cross-bedding	Well- to medium-rounded and sorted; 50–10 $\mu\text{m}$	Intertidal-shoal setting, shoreface
(Lf-5) Stromatolite mudstone	Micrite, algae	Ripple lamination	<50 $\mu\text{m}$	Shallow subtidal, shoreface
(Lf-6) Pisolitic grainstone	Peloids, ooids, pisoids, spherulites, algae, trilobites	Hummocky cross-bedding	Poorly sorted and medium- to poorly rounded, 0.1–5 mm	Barrier or buildup, upper offshore
(Lf-7) Algal boundstone	Peloids, ooids, spherulites, algae, trilobites	Massive structure	<50 $\mu\text{m}$	Barrier, buildup, upper offshore
(Lf-8) Oncolitic rudstone	Oncolite, quartz, marls, ooids, algae	Grading-bedding, erosional surface	Finely sorted and finely rounded, 10–1 mm	Storm deposits, upper offshore
(Lf-9) Interclast packstone	Breccia, peloids, micrite, marls, trilobites	Massive structure, imbrication	Medium-rounded and well-sorted; 5–1 mm	Upper offshore
(Lf-10) Radial spheroid packstone	Radial spherulites, ooids, micrite, marls, trilobites, quartz	Trough to ripple cross-bedding	Well to moderately rounded, moderately sorted, 0.1–1 mm	Storm deposits, upper offshore
(Lf-11) Trilobite-sponge spicule wackestone	Peloids, trilobites, sponge spicules	Massive structure	Poorly sorted and very fine granule, 10–60 $\mu\text{m}$	Lower offshore
(Lf-12) Marl mudstone	Quartz, marls, trilobites, sponge spicule	Structureless	Fine granule, <50 $\mu\text{m}$	Lower offshore
(Lf-13) Shale mudstone	Muds	Lamination	Fine granule, <50 $\mu\text{m}$	Lower offshore

grain to rudstone texture (Figure 4A). The pisoids are noteworthy for their broad range of diameters (0.5 to 4.0 cm). The interparticle porosity is filled with microspar calcite cement, with occasional infilling by mud and small clasts. Cross-bedding in this unit is hummocky (Figure 4B), which indicates deposition below the fair-weather wave base, but with episodic influence by storm-driven hydrodynamics (Carpentier et al., 2010). Lf-6 is commonly associated with Lf-3, Lf-4, and Lf-5, as well as Lf-8 and Lf-11.

The algal boundstone (Lf-7) primarily consists of bulbous algae, as reported by Read and Pfeil (1983) and Kobluk (1986), in Laurentia during the Cambrian Period (Figures 4C, D). The skeletal algae are primarily composed of Epiphyton (Figure 4C), a protozoan that typically occupies low-to-moderate energy settings, as encountered between fair-weather and storm-weather wave bases (Della Porta et al., 2004). According to previous studies in the Cambrian Period (Barnaby and Read, 1990; Read and Pfeil, 1983), this facies has the potential to constitute a buildup/barrier with relatively high relief, as may typify the margin of a rimmed platform. Lf-7 mainly develops in regressive successions, but occasionally appears in transgressive successions. Lf-7 is associated with Lf-9 and Lf-11.

Occurring in massive beds with rudstone texture, Lf-8 is an oncolitic rudstone commonly associated with regressive, and occasionally transgressive, successions (Figure 4E). Individual oncoids range in size from 1 to 10 mm (Figure 4F). These units are interleaved with planar mudstone intervals with up to 20-cm thickness. Evidence for erosional surfaces appears within Lf-8 with mm- to cm-scale relief, indicating episodic storm-induced influence. Those associated with this lithofacies are Lf-4, Lf-8, and Lf-11. The rate of sedimentation in this lithofacies was presumed to be low on the basis of micritic cortices observed around the oncoids (Flügel, 2010). Furthermore, the frequent presence of intraclasts and micritized ooids (likely wash-over deposits) suggests that Lf-7 is situated in close proximity to an ooid-producing area.

The intraclast packstone/wackestone (Lf-9) commonly occurs as a packstone to wackestone fabric in the form of imbricated breccia, likely related to channel sediments, with poor-sorting and partially rounded intraclasts, set within a mud-rich micritic matrix (Figures 4G, H). The environment of deposition of Lf-9 was interpreted to be the most distal portion of the offshore sediments, although still influenced by river inputs (Andrieu et al., 2016). This lithofacies is associated with Lf-6 and Lf-8, and

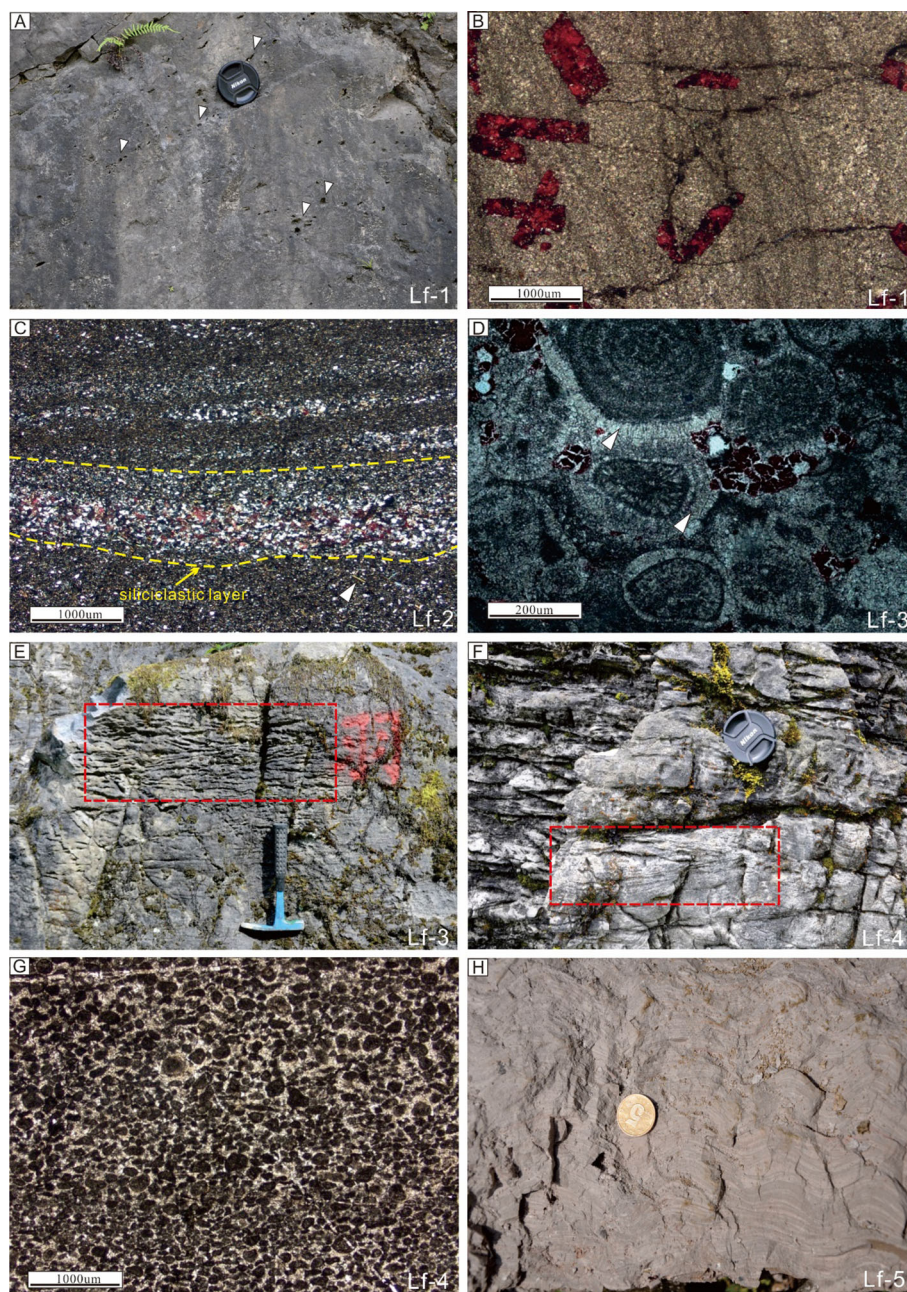


**FIGURE 3**

Characteristic shoreface lithofacies as resolved in outcrop and thin sections. (A, B) Lf-1. White arrows in panel A emphasize fenestrate structures, while panel B shows moldic porosity filled with microspar calcite cement (Gaodongmiao Section; plane-polarized light). (C) Lf-2, which is characterized by laminated quartz and mica (white arrow) in a sandy mudstone (Bancun Section; cross-polarized light). (D, E) Aspects of Lf-3, an ooid grainstone containing concentric ooids coated with fibrous cement (white arrow in panel D) (Yangjiaping Section; plane-polarized light) and herringbone cross-bedding (E). Lf-4 is a cross-bedded peloidal packstone to grainstone (Tuhe Section, F). Grains are rounded and medium- to well-sorted (G). (H) Lf-5, a stromatolitic mudstone.

Lf-10 and Lf-11. Lf-9 was recognized in both regressive and transgressive sequences.

The radial spheroid packstone (Lf-10) is the marker horizon of the first transgression at the beginning of the Longwangmiao Fm (Tan et al., 2017). This lithofacies is characterized by abundant radial spheroids with little internal structure. These grains are well-

to moderately rounded and moderately sorted. Their sizes range from 0.1 to 1.5 mm (Figure 4I). Some intraclasts, consisting of debris such as trilobite fragments and terrigenous quartz, were readily identified in a micritic matrix. The radial spheroids within Lf-10 are equivalent to those reported by Strasser (1986), which were presumed to have developed in a shallow microbial-rich

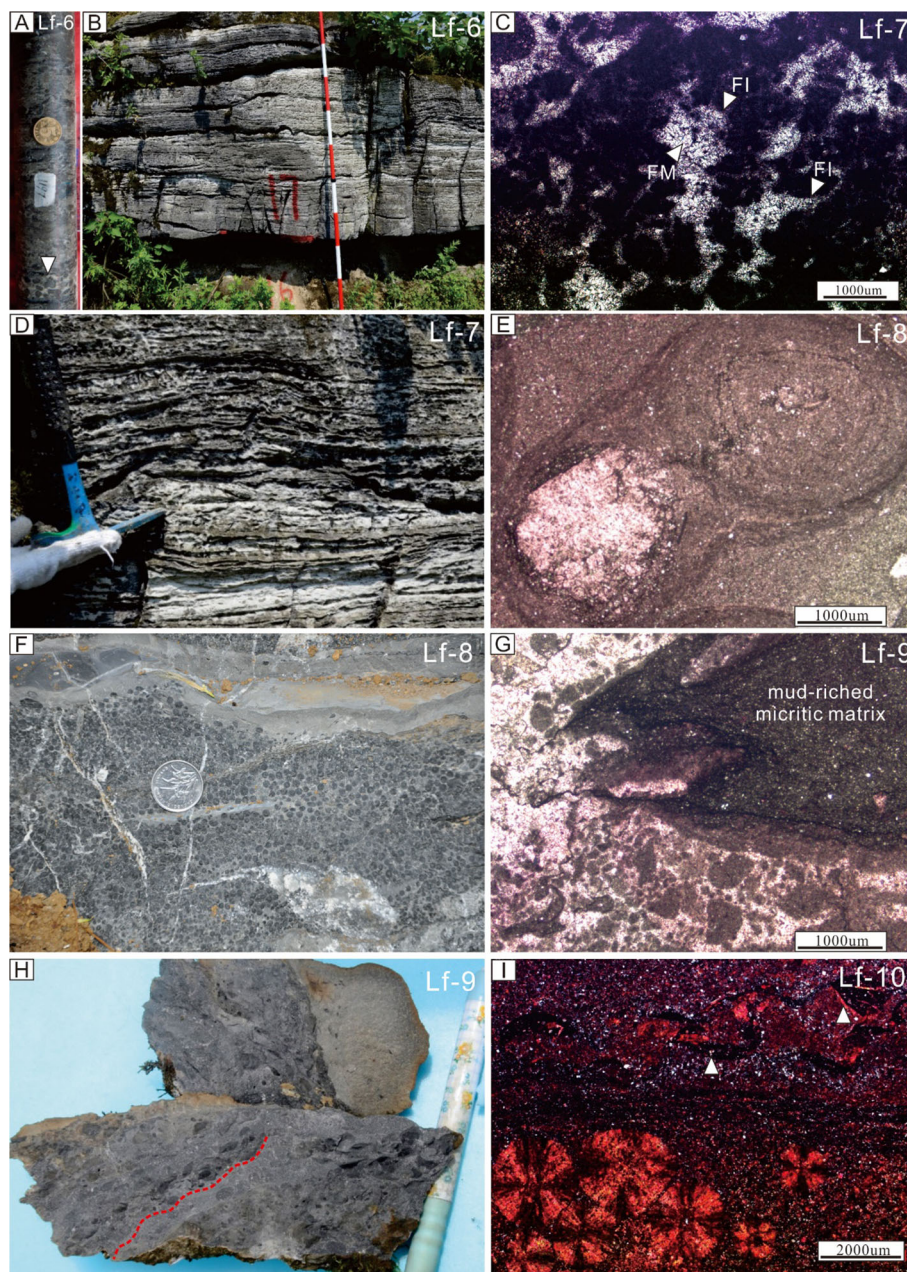


FIGURE 4

Characteristic upper-shoreface lithofacies as resolved in outcrop and thin sections. (A, B) Lf-6. The core in (A) shows loosely stacked pisolites (white arrow) in Lf-6 (Well YD2, 1,208 m below ground level). Cross-bedding in Lf-6 is hummocky (B). (C) Calcareous algae (Epiphyton) appeared in Lf-7. Abundant pores and cavities are infilled with recrystallized fibrous (FI) and fine- to medium-crystal (FM) calcite cement (Tuhe Section, plane-polarized light). (D) Lf-7 shows the mound shape (Tuhe Section). (E) Lf-8 emphasizes the oncolites and thin mudstone interbeds (Songlin Section). (F) The two oncolites are coated with micritic cortices in the micritic matrix (Songlin Section, plane-polarized light). (G, H) Lf-9. (G) The intraclast and bioclast sediments cut and infill the micritic matrix. (H) An imbricated breccia (red dash line) floating in a micritic matrix as viewed in Lf-9 (Gaodongmiao Section). (I) Radial spheroids and trilobite clasts (white arrow) in Lf-10 (Bancun Section, cross-polarized light).

environment with varying water energy and high oxygenation (e.g., Tan et al., 2017). This lithofacies is commonly associated with Lf-4, Lf-6, Lf-9, and Lf-11.

#### 4.1.3 Lower-offshore lithofacies (Lf-11 through Lf-13)

Dominant grain types in the trilobite–sponge spicule wackestone (Lf-11) are, as the name suggests, sponge spicules and

trilobite fragments (Figure 5A). This faunal assemblage was interpreted to be an open marine setting situated between fair- and storm-weather wave bases (Wyn and Hughes, 2004). An equivalent assemblage in the Lower Saxony Basin reported by Kästner et al. (2008) was interpreted to be a middle ramp setting. The presence of mud in this lithofacies suggests a low-energy depositional environment. This lithofacies is frequently associated with Lf-6, Lf-8, and Lf-9.

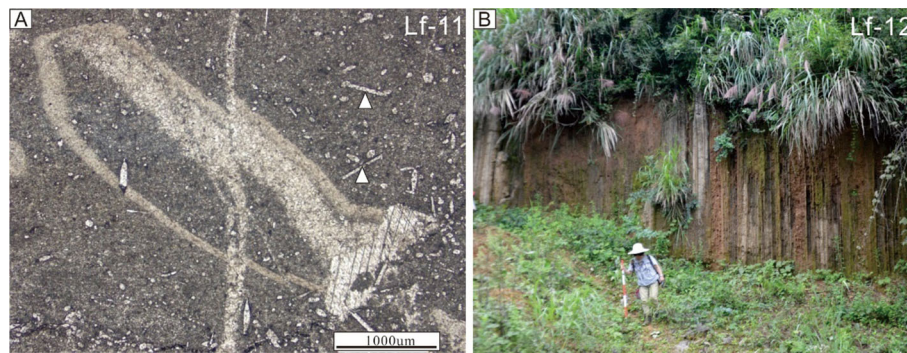


FIGURE 5

Characteristic lower-shoreface lithofacies as resolved in outcrop and thin sections. (A) Sponge spicules (white arrows) and trilobite fragments identified in Lf-11 (Nanshanping Section, plane-polarized light). (B) The thin marl mudstone layer interbeds within shales in the lower offshore environment (Nanshanping Section).

The marl mudstone (Lf-12) and shale mudstone (Lf-13) suggest an outer ramp environment, likely situated beneath the storm wave base. Lf-12 occurs as thin (5–15 cm thick) evenly bedded units that are devoid of any bioclastic materials or sedimentary structure, save for rare, fine parallel laminations (Figure 5B). Those lithofacies were observed in transgressive sequences and are associated with Lf-11 and Lf-8.

#### 4.1.4 Sequence stratigraphic surface

Most of the sequence stratigraphic boundaries are composed of changes in lithological associations. The top surface of the Longwangmiao Formation is characterized by iron-rich oxides and eogenetic karst, which shows the dissolution of grain-packstone and directly overlies the mudstone of the Gaotai Formation (Figures 6A, B). The top boundary of SQ2 was also recognized in the Bancun Section and shows the subaerial exposure surface of the sandy mudstone. The transition of lithological facies from peloidal grainstone/packstone, associated with dissolved pore, to intraclast wackestone is a depositional hiatus and can be regarded as the boundary between SQ1 and SQ2 (Figure 6C).

## 4.2 Geochemistry

### 4.2.1 Stable carbon and oxygen isotopes

In the Bancun Section, the average values of  $\delta^{13}\text{C}$  and  $\delta^{18}\text{O}$  are  $-0.96\text{‰}$  (SD = 1.26‰) and  $-8.95\text{‰}$  (SD = 1.58), respectively. The vertical trend of  $\delta^{13}\text{C}$  values shows that two negative excursions correlate to the top surface of PSQ4 (LNE2) and the transition from PSQ2 to PSQ3 (LNE1) (Figure 7). Three positive fluctuations of  $\delta^{18}\text{O}$  values are identified, decoupling with the variation of  $\delta^{13}\text{C}$  values. The frequently varying trends of  $\delta^{13}\text{C}$  (mean value =  $-0.84\text{‰}$ , SD = 1.68‰) and  $\delta^{18}\text{O}$  values (mean value =  $-8.16\text{‰}$ , SD = 1.85) are displayed in the Gaodongmiao Section. The largest negative excursion of  $\delta^{13}\text{C}$  is located in the top part of PSQ4. Another excursion is located along the boundary between PSQ2 and PSQ3, which has a negative trend as was observed in the Bancun Section. In the Tuhe Section (Figure 8), the vertical variations of

$\delta^{13}\text{C}$  (mean value =  $-0.42\text{‰}$ , SD = 1.95‰) and  $\delta^{18}\text{O}$  values (mean value =  $-8.93\text{‰}$ , SD = 1.44) are similar to those in the Bancun Section with two negative excursions of  $\delta^{13}\text{C}$  at the top part of PSQ4 and the boundary between PSQ2 and PSQ3. In contrast, the largest negative excursion of  $\delta^{13}\text{C}$  is located during the transition from PSQ2 to PSQ3 in the Yankong Section. The covariation between  $\delta^{13}\text{C}$  and  $\delta^{18}\text{O}$  values is ambiguous (Figure 9A). The Mn/Sr ratios range from 0.23 to 5.60, and the correlation between Mn/Sr and  $\delta^{18}\text{O}$  values is also weak (Figure 9B).

### 4.2.2 Chemical Index of Alteration

The CIA was derived for three of the nine examined outcrops. The CIA values calculated using Equation 1 ranged from 62 to 100 (mean value = 80, and SD = 9) (Figure 10), indicating disparate degrees of weathering. In the Bancun Section, a positive shift in the CIA from 64 to 89 (mean value = 77 and SD = 6) was recognized during the transition from PSQ2 to PSQ3. A comparable shift was also seen in the Gaodongmiao and Yankong Sections at the same sequence boundaries, and their CIA values ranged from 62 to 100 and 64 to 91, respectively.

## 5 Discussion

### 5.1 Sequence stratigraphic framework and platform evolution

The transgressive–regressive sequence model was used to construct the sequence stratigraphic framework, bounded by subaerial exposure surfaces and subdivided into transgressive and regressive packages by the maximum flooding surface (Catuneanu, 2022; Embry, 1993). The changes in facies stacking and abrupt lithofacies shifts mark subordinate surfaces (Jiang et al., 2002; Lan et al., 2022). Two sequences were identified: the first sequence (SQ1) contains PSQ1 and PSQ2, while the second sequence (SQ2) contains PSQ3 through PSQ6 (Figure 6).

In PSQ1, the stratigraphic thickness and facies architecture show a pronounced variation between the northern and southern



FIGURE 6

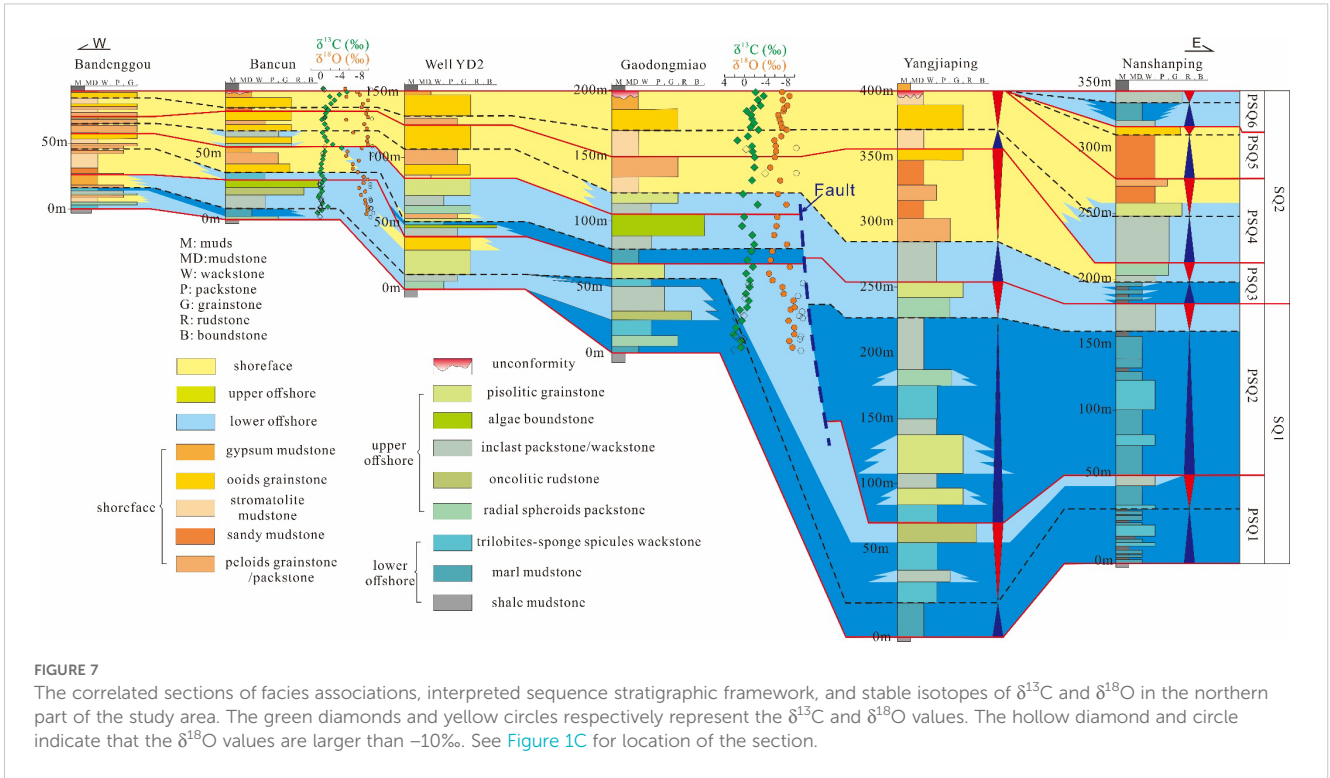
Photos of stratigraphic interfaces. (A, D) Top surface of SQ2 in GDM and BC. (B, C) The interface of SQ1 and SQ2. GDM, Gaodongmiao Section; BC, Bancun Section.

parts of the study area (Figures 7, 8). In the north, the thickness of the succession is characterized by a gently increasing trend from west to east, suggesting a low-angle ramp morphology (Figure 7). In contrast, the strata showed a dramatically decreasing thickness basinward in the southern part of the study area (Figure 8). Here, it should be noted that the Meiziwan Section is thinner than neighboring logged sections (e.g., Tuhe and Yankong) because the underlying Canglangpu Fm. is stratigraphically elevated in this area. During the transgression, the subtabular-to-undulate, bioclast-rich, radial spheroidal packstone (Lf-10) widely developed on the platform top, which represents a marker horizon (Tan et al., 2017). In the subsequent regressive system, ooid shoals (Lf-3) locally develop in the study area. Available evidence points to the fact that the platform adopted the morphology of a low-angle (homoclinal) ramp during PSQ1 (Figure 11A), although some localized topographic relief was present (as observed in the Meiziwan Section; Figure 8).

In PSQ2, the Yangjiaping and Zhenyuan Sections demarcating the transition from the upper to lower offshore display a dramatic thickening (Figures 7, 8). This increase in thickness is sufficiently

large to suggest the presence of a fault, with both the Yangjiaping and Zhenyuan Sections situated on its footwall. Both sections display a wide variety of facies successions that correspond to lower offshore facies (Lf-11 and Lf-12) and upper offshore facies (Lf-6, Lf-9, and Lf-10). The adjacent Gaodongmiao and Meiziwan Sections, meanwhile, were interpreted to sit on the hanging wall of the fault, and the associated depositional relief resulted in the development of buildup and barrier successions (Lf-6 and Lf-7). The presence of the fault caused the platform morphology to evolve from a homocline in PSQ1 to a distally steepened ramp in PSQ2 (Figure 11B).

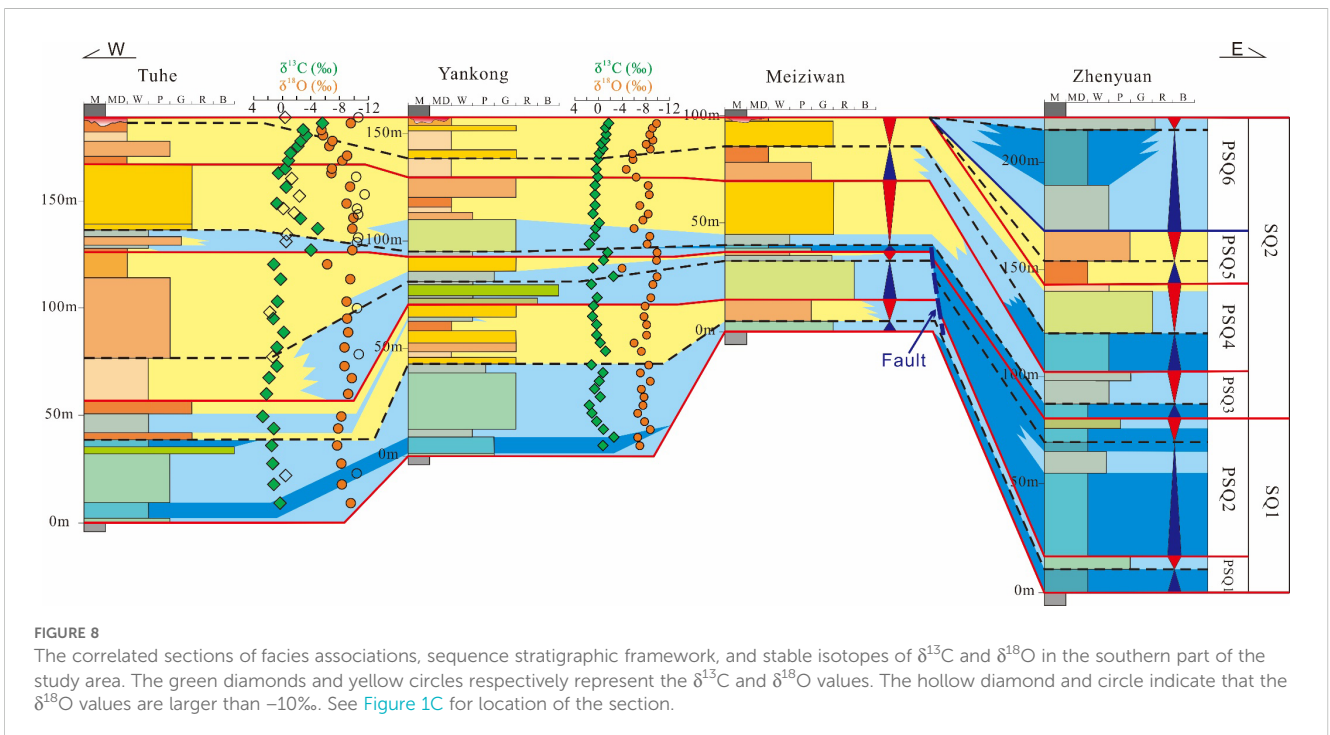
Whereas PSQ1 and PSQ2 display a diversity of deep- and shallow-water facies, PSQ3 by contrast is dominated by a platform-top depositional system. The facies associations are encompassed by Lf-2 through Lf-5, and the thickness of the sequence is thicker around the marginal platform (e.g., Yangjiaping Section). The logged sections indicate the widespread development of high-energy ooid shoals, particularly in the vicinity of the platform margin (Lf-3 and Lf-4), which is locally interbedded with sandy mudstone (Lf-2) and other low-energy facies (e.g., Lf-9



and Lf-10). Such interbedding suggests meaningful variation in water depth. Previous studies (e.g., Gao et al., 1991; Liu et al., 1987) have proposed that the existence of PSQ3 gravity deposits seaward of the platform margin developed in deep water on the foreslope. The presence of gravity deposits via mass wasting of the platform margin suggests that the shelf break has been relatively steep. All evidence considered, the platform seems to have evolved from a

distally steepened ramp in PSQ2 to a rimmed platform with a defined shelf break in PSQ3 (Figure 11C).

Moving up-section, PSQ4 is also dominated by shallow-water deposits, save for its most distal reaches (i.e., the Nanshanping and Zhengyuan Sections), which preserve deep-water facies. Sections penetrating the shallow-water successions are dominated by grain-rich peritidal deposits (Lf-1 through Lf-5). PSQ4 is capped by a



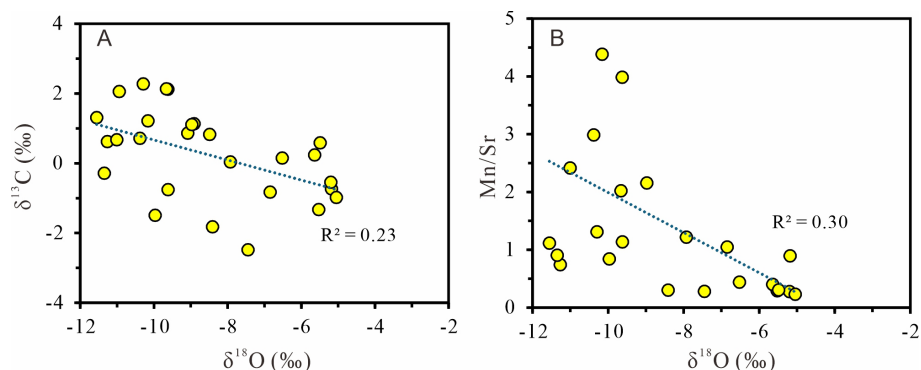


**FIGURE 9** Cross-plots of (A) between  $\delta^{13}\text{C}$  and  $\delta^{18}\text{O}$  values and (B) between Mn/Sr and  $\delta^{18}\text{O}$  values for dolomites from the Longwangmiao Formation (data from Lu et al., 2025).

well-defined exposure surface in all sections, except Nanshanping and Zhengyuan, both of which are characterized by deep-water facies (Figures 7, 8). At the base of PSQ4, the topography of the platform clearly follows that inherited from the previous parasequence. However, at the top of PSQ4, the platform was interpreted to have further evolved to a flat-topped form (Figure 11D). The morphology is considered to be similar to that reported in Sequence III of the Lower Mississippian Madison Limestone of Wyoming (Smith et al., 2004).

Finally, PSQ5 and PSQ6 are not represented in the majority of logged sections, but only in those situated in the most distal locations—the Nanshanping and Zhengyuan Sections (Figures 7, 8). Here, PSQ5 is dominated by shoreface facies (Lf-2 through Lf-4), but in

PSQ6, the logged facies are indicative of deep-water, low-energy upper and lower offshore facies (Lf-9 and Lf-11). The fact that PSQ5 and PSQ6 are absent in the more proximal sections (which in turn are capped by an exposure surface) suggests that the transgressions were of insufficient magnitude to flood the platform top.

### 5.2 Transition from ramp to rimmed platform

The stratigraphic reconstruction of the Yangtze Platform developed herein suggests evolution from a ramp to a rimmed platform during the transition from PSQ2 to PSQ3 (Figures 11B, C).

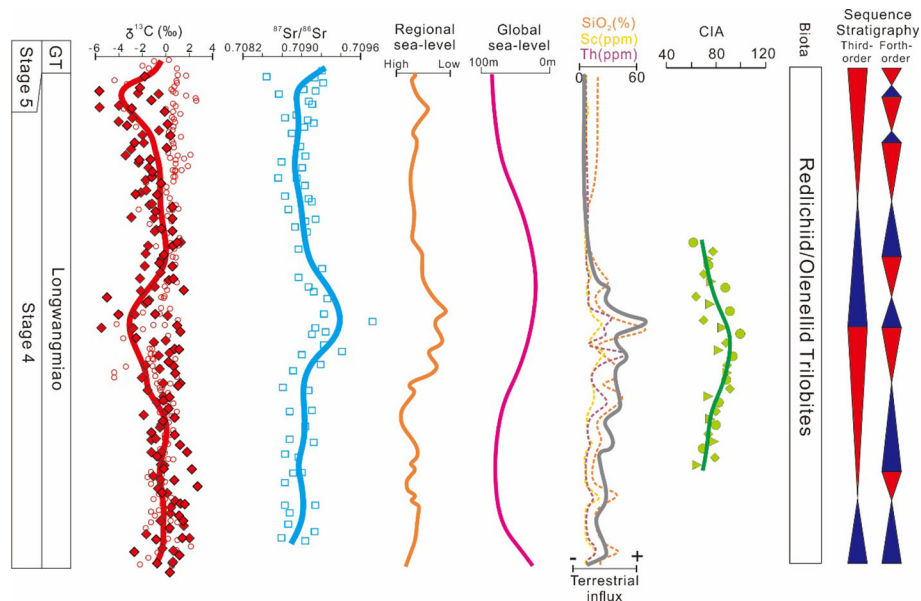
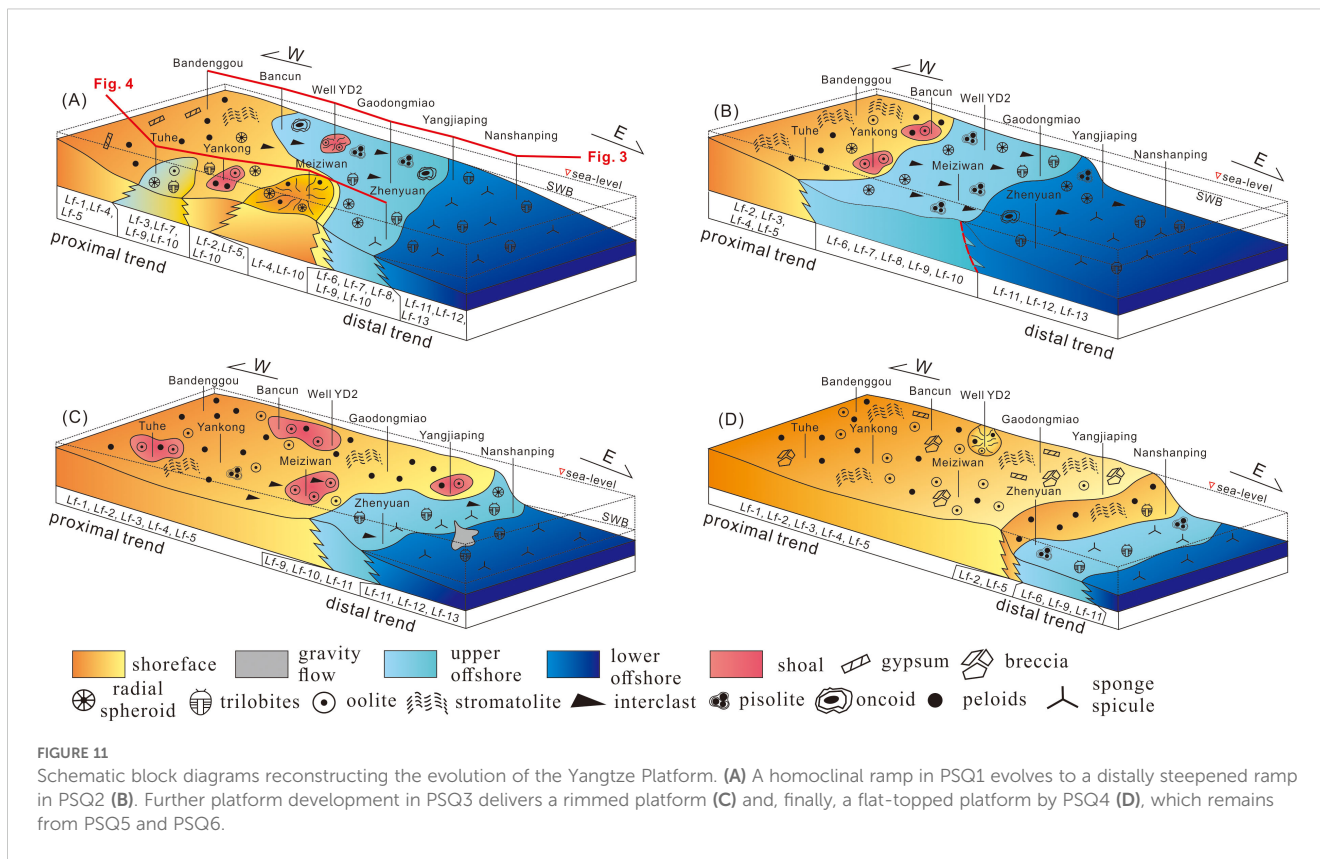


**FIGURE 10** Comparison of C isotope, Sr isotope, CIA ratio, terrestrial influx, relative and global sea levels, and sequence stratigraphy of the Yangtze Block. The carbon isotope data are from shallow-water sections of Ma et al. (2015), Ren et al. (2017), Yang et al. (2017), Lu et al. (2018), and this study. The strontium isotope data are from Burke et al. (1982), Keto and Jacobsen (1987), Gao et al. (1991), Derry et al. (1994), and Huang et al. Locations are shown in Figures 1A, C. The regional sea-level and global sea-level curves are from Ren et al. (2017) and Haq and Schutter (2008). The terrestrial influx, including the contents of  $\text{SiO}_2$ , Sc, and Th, are from Ren et al. (2019). CIA, Chemical Index of Alteration.



This change in geometry is associated with depleted  $\delta^{13}\text{C}$  values in the associated sediments and a positive shift in the CIA (Figure 10). The CIA in the insoluble component of carbonate sediments can be applied to evaluate the weathering history of the deposit (Nesbitt, 1979; Nesbitt and Young, 1982). In general, intense chemical weathering corresponds to a high CIA ratio (Yang et al., 2016). Our interpretation of increased weathering across the PSQ2–3 boundary is corroborated by compiled Sr isotope data (Figure 10). Further evidence came from Ren et al. (2018), who reported an increase in terrestrial detritus on the Yangtze Platform in the same time period. The sea-level curve of Haq and Schutter (2008) suggested that the increase in chemical weathering is accompanied by a pronounced fall in sea level, likely resulting from forcing the change in geometry from a ramp to a rimmed platform (Pomar and Haq, 2016).

The transition across the PSQ2–PSQ3– boundary (LNE1) is marked by a pronounced negative  $^{13}\text{C}$  excursion (Figure 10). There are three plausible explanations for this trend: the first is that the poor circulation of water masses was accompanied by an effect of “seawater aging”, which is the epicontinental water masses and restricted circulation between epicontinental and oceanic environments, and seawater aging leads to a negative excursion in  $\delta^{13}\text{C}$ , mainly due to the decomposition of organic carbon in seawater over time, which produces  $\text{CO}_2$ -enriched  $^{12}\text{C}$ , resulting in a decrease in the  $^{13}\text{C}/^{12}\text{C}$  ratio in dissolved inorganic carbon (DIC) in seawater, which is ultimately manifested as a

decrease in the  $\delta^{13}\text{C}$  value (e.g., Holmden et al., 1998). The second explanation is that riverine input, associated with the sea level drop, transported depleted  $^{13}\text{C}$  to the system (e.g., Immenhauser et al., 2003). Excess nutrients leading to biomass extinction is the third explanation for the negative  $^{13}\text{C}$  excursion. Under this scenario, primary production would drastically reduce, leading to a reduced burial rate for organic matter (e.g., Ren et al., 2017).

If the LNE1 negative  $^{13}\text{C}$  excursion is attributed to riverine influence, the lateral variation of  $\delta^{13}\text{C}$  values should display a decreasing gradient from the proximal platform to the distal platform. However, such a trend is not supported by the data (Figures 7, 8 and Supplementary Tables S1–S3). Furthermore, given that land plants have yet to evolve, Cambrian rivers may not be expected to be meaningfully depleted in  $^{13}\text{C}$ . Excess nutrients and biomass extinction are also insufficient to explain the LNE1 because, unlike the observations of Ren et al. (2017), trilobite fossils were recognized in the upper part of Stage 4 (the Longwangmiao Fm.) in different sections from the shallow to deep setting of the Yangtze Platform (Chang et al., 2017; Zhu et al., 2006; Zuo et al., 2018). By process of elimination, and the weak correlation between  $\delta^{18}\text{O}$  and  $\delta^{13}\text{C}$ , Mn/Sr, the most plausible explanation for the LNE1 excursion is that it was induced by water mass restriction associated with the transition in platform geometry. The term “seawater aging” indicates that the occurrence of more negative  $\delta^{13}\text{C}$  values was caused by the

progressive oxidation of organic matter to CO<sub>2</sub> during long platform-top residence times (Holmden et al., 1998; Immenhauser et al., 2003).

## 6 Conclusion

The Longwangmiao Fm. consists of 13 lithofacies encompassing three facies associations (shoreface, upper offshore, and lower offshore). Two third-order sequences (SQ1 and SQ2) and six fourth-order sequences (PSQ1–PSQ6) were interpreted in the study. Platform geometry was observed to evolve from a homoclinal ramp (PSQ1) to a distally steepened ramp (PSQ2), then to a rimmed platform (PSQ3), and finally to a flat-topped platform (PSQ4, PSQ5, and PSQ6). The transition from ramp to rimmed geometry occurs at the time of transition from PSQ2 to PSQ3. This change in geometry is accompanied by enhanced terrestrial influx and the depletion of δ<sup>13</sup>C (LNE1). Enhanced terrigenous detritus influx, coupled with the prolonged retention and oxidation of organic matter on platform tops generating CO<sub>2</sub>-induced “seawater aging”, manifested as δ<sup>13</sup>C depletion (LNE1), collectively driving carbonate platform evolution. The results provide an example of how the combined application of geochemical techniques within a sequence stratigraphic framework better constrains the evolution of carbonate platforms.

## Data availability statement

The original contributions presented in the study are included in the article/Supplementary Material. Further inquiries can be directed to the corresponding author.

## Author contributions

GW: Writing – original draft, Writing – review & editing. HG: Writing – review & editing. HZ: Writing – review & editing.

## References

- Andreucci, S., Pistis, M., Funedda, A., and Loi, A. (2017). Semi-isolated, flat-topped carbonate platform (Oligo-Miocene, Sardinia, Italy): Sedimentary architecture and processes. *Sedimentary Geology* 361, 64–81. doi: 10.1016/j.sedgeo.2017.09.012
- Andrieu, S., Brigaud, B., Barbarand, J., Lasseur, E., and Saucède, T. (2016). Disentangling the control of tectonics, eustasy, trophic conditions and climate on shallow-marine carbonate production during the Aalenian–Oxfordian interval: From the western France platform to the western Tethyan domain. *Sedimentary Geology* 345, 54–84. doi: 10.1016/j.sedgeo.2016.09.005
- Barnaby, R. J., and Read, J. F. (1990). Carbonate ramp to rimmed shelf evolution: Lower to Middle Cambrian continental margin, Virginia Appalachians. *Geological Soc. America Bull.* 102, 391–404. doi: 10.1130/0016-7606(1990)102<0391:CRTRSE>2.3.CO;2
- Bover-Arnal, T., Salas, R., Moreno-Bedmar, J. A., and Bitzer, K. (2009). Sequence stratigraphy and architecture of a late Early–Middle Aptian carbonate platform succession from the western Maestrat Basin (Iberian Chain, Spain). *Sedimentary Geology* 219, 280–301. doi: 10.1016/j.sedgeo.2009.05.016
- Brigaud, B., Durlot, C., Deconinck, J.-F., Vincent, B., Pucéat, E., Thierry, J., et al. (2009). Facies and climate/environmental changes recorded on a carbonate ramp: A sedimentological and geochemical approach on Middle Jurassic carbonates (Paris Basin, France). *Sedimentary Geology* 222, 181–206. doi: 10.1016/j.sedgeo.2009.09.005
- Burke, W. H., Denison, R. E., Hetherington, E. A., Koepnick, R. B., Nelson, H. F., Otto, J. B., et al. Variation of seawater 87Sr/86Sr throughout Phanerozoic time. *Geology* 1982 10(10), 516–519. doi: 10.1130/0091-7613(1982)10<516:VOSSTP>2.0.CO;2
- Carpentier, C., Lathuilière, B., and Ferry, S. J. S. (2010). Sequential and climatic framework of the growth and demise of a carbonate platform: implications for the peritidal cycles (Late Jurassic, North-eastern France). *Sedimentology*. 57, 985–1020. doi: 10.1111/j.1365-3091.2009.01128.x
- Catuneanu, O. (2022). “Chapter 8 - Variability of stratigraphic sequences,” in *Principles of Sequence Stratigraphy (Second Edition)*. Ed. O. Catuneanu (Elsevier, Amsterdam), 337–388.
- Chang, C., Hu, W., Wang, X., Yu, H., Yang, A., Cao, J., et al. (2017). Carbon isotope stratigraphy of the lower to middle Cambrian on the eastern Yangtze Platform, South

## Funding

The author(s) declare that financial support was received for the research and/or publication of this article. This study was supported by the Special Funds for Taishan Scholars Program (tsqn202211073), the mechanism of formation and preservation of ultra-deep carbonate reservoirs (P24246) supported by Sinopec Group.

## Conflict of interest

The authors declare that this study received funding from the Sinopec Group. The funder had the following involvement in the study: data collection and analysis.

## Generative AI statement

The author(s) declare that no Generative AI was used in the creation of this manuscript.

## Publisher’s note

All claims expressed in this article are solely those of the authors and do not necessarily represent those of their affiliated organizations, or those of the publisher, the editors and the reviewers. Any product that may be evaluated in this article, or claim that may be made by its manufacturer, is not guaranteed or endorsed by the publisher.

## Supplementary material

The Supplementary Material for this article can be found online at: <https://www.frontiersin.org/articles/10.3389/fmars.2025.1607571/full#supplementary-material>

- China. *Palaeogeography Palaeoclimatology Palaeoecol.* 479, 90–101. doi: 10.1016/j.palaeo.2017.04.019
- Chen, D., Yang, B., Song, Y., Guo, C., Zhou, X., Wang, Y., et al. (2024). Depositional facies and evolution of sponge-microbial-constructed carbonate platforms in the lower Cambrian (Stage 3), Tarim basin, China: Understanding from anatomy. *Mar. Petroleum Geology* 167, 106957. doi: 10.1016/j.marpetgeo.2024.106957
- Della Porta, G., Kenter, J. A. M., and Bahamonde, J. R. (2004). Depositional facies and stratal geometry of an Upper Carboniferous prograding and aggrading high-relief carbonate platform (Cantabrian Mountains, N Spain). *Sedimentology* 51, 267–295. doi: 10.1046/j.1365-3091.2003.00621.x
- Derry, L. A., Brasier, M. D., Corfield, R. M., Rozanov, A. Y., and Zhuravlev, A. Y. (1994). Sr and C isotopes in Lower Cambrian carbonates from the Siberian craton: A paleoenvironmental record during the 'Cambrian explosion'. *Earth and Planetary Science Letters*, 128, 671–681.
- Di Lucia, M., Sayago, J., Frijia, G., Cotti, A., Sitta, A., and Mutti, M. (2017). Facies and seismic analysis of the Late Carboniferous–Early Permian Finnmark carbonate platform (southern Norwegian Barents Sea): An assessment of the carbonate factories and depositional geometries. *Mar. Petroleum Geology* 79, 372–393. doi: 10.1016/j.marpetgeo.2016.10.029
- Du, J., Zhang, B., Wang, Z., Zou, C., Xu, C., Shen, P., et al. (2016). Sedimentary mode and reservoir genesis of dual grain banks at the Lower Cambrian Longwangmiao Fm carbonate ramp in the Sichuan Basin. *Natural Gas Industry B* 3, 399–408. doi: 10.1016/j.ngib.2017.02.001
- Erick, M. (1996). Sequence stratigraphy and platform evolution of Lower–Middle Devonian carbonates, eastern Great Basin. *GSA Bull.* 108, 392–416. doi: 10.1130/0016-7606(1996)108<0392:SSAPEO>2.3.CO;2
- Embry, A. F. (1993). Transgressive–regressive (T–R) sequence analysis of the Jurassic succession of the Sverdrup Basin, Canadian Arctic Archipelago. *Can. J. Earth Sci.* 30, 301–320. doi: 10.1139/e93-024
- Embry, A. F., and Klovan, J. E. (1971). A late Devonian reef tract on northeastern Banks Island, NWT. *Bull. Can. Petroleum Geology* 19, 730–781. doi: 10.35767/gscpgbull.19.4.730
- Fallatah, M. I., and Kerans, C. (2018). Stratigraphic evolution of the Late Jurassic Hanifa Formation along the Tuwaiq Escarpment, Saudi Arabia: Evidence for a carbonate ramp system. *Sedimentary Geology* 363, 152–180. doi: 10.1016/j.sedgeo.2017.10.008
- Flügel, E. (2010). *Microfacies of Carbonate Rocks, Analysis, Interpretation and Application* (Berlin: Springer-Verlag, Springer), 976.
- Friedman, I., and O'Neil, J. R. (1977). *Data of geochemistry: Compilation of stable isotope fractionation factors of geochemical interest* (US Government Printing Office).
- Guo, Q., Strauss, H., Liu, C., Zhao, Y., Yang, X., Peng, J., et al. (2010). A negative carbon isotope excursion defines the boundary from Cambrian Series 2 to Cambrian Series 3 on the Yangtze Platform, South China. *Palaeogeography Palaeoclimatology Palaeoecol.* 285, 143–151. doi: 10.1016/j.palaeo.2009.11.005
- Gao, G., and Land, L. S. (1991). Land, Geochemistry of Cambro-Ordovician Arbuckle limestone, Oklahoma: Implications for diagenetic  $\delta^{18}\text{O}$  alteration and secular  $\delta^{13}\text{C}$  and  $87\text{Sr}/86\text{Sr}$  variation. *Geochimica et Cosmochimica Acta*, 55, (10), 2911–2920. doi: 10.1016/0016-7037(91)90456-F
- Hallock, P., and Schlager, W. (1986). Nutrient excess and the demise of coral reefs and carbonate platforms. *Palaios* 1, 389–398. doi: 10.2307/3514476
- Haq, B. U., and Schutter, S. R. (2008). A chronology of paleozoic sea-level changes. *Science* 322, 64–68. doi: 10.1126/science.1161648
- Holmden, C., Creaser, R., Muehlenbachs, K., Leslie, S., and Bergstrom, S. (1998). Isotopic evidence for geochemical decoupling between ancient epeiric seas and bordering oceans: implications for secular curves. *Geology* 26, 567–570. doi: 10.1130/0091-7613(1998)026<0567:IEFGDB>2.3.CO;2
- Huang, F. X., Chen, H. D., Hou, M. C., Zhong, Y. J., Jie, and Li. (2011). Filling process and evolutionary model of sedimentary sequence of Middle-Upper Yangtze craton in Caledonian (Cambrian–Silurian). *Acta Petrologica Sin.* 27, 2299–2317.
- Immenhauser, A., Della Porta, G., Kenter, J. A. M., and Bahamonde, J. R. (2003). An alternative model for positive shifts in shallow-marine carbonate  $\delta^{13}\text{C}$  and  $\delta^{18}\text{O}$ . *Sedimentology* 50, 953–959. doi: 10.1046/j.1365-3091.2003.00590.x
- Jiang, G., Christie-Blick, N., Kaufman, A. J., Banerjee, D. M., and Rai, V. (2002). Sequence stratigraphy of the neoproterozoic infra krol formation and krol group, lesser himalaya, India. *J. Sedimentary Res.* 72, 524–542. doi: 10.1306/120301720524
- Jin, X., Shi, Z., Rigo, M., Franceschi, M., and Preto, N. (2018). Carbonate platform crisis in the Carnian (Late Triassic) of Hanwang (Sichuan Basin, South China): Insights from conodonts and stable isotope data. *J. Asian Earth Sci.* 164, 104–124. doi: 10.1016/j.jseas.2018.06.021
- Jin, X., Song, J., Liu, S., Li, Z., Yang, D., and Wang, H. (2025). Three-terraced evaporated ramp model for differentiation of the massive dolomitization process: Insights from the Lower Cambrian Longwangmiao Formation in the Sichuan Basin. *Adv. Geo-Energy Res.* 15, 216–229. doi: 10.46690/ager.2025.03.05
- Kästner, M., Schülke, I., and Winsemann, J. (2008). Facies architecture of a Late Jurassic carbonate ramp: the Korallenolith of the Lower Saxony Basin. *Int. J. Earth Sci.* 97, 991–1011. doi: 10.1007/s00531-007-0282-z
- Kelley, B. M., Lehrmann, D. J., Yu, M., Minzoni, M., Enos, P., Li, X., et al. (2017). The Late Permian to Late Triassic Great Bank of Guizhou: An isolated carbonate platform in the Nanpanjiang Basin of Guizhou Province, China. *AAPG Bull.* 101, 553–562. doi: 10.1306/011817DIG17034
- Keto, L. S., and Jacobsen, S. B. (1987). Nd and Sr isotopic variations of Early Paleozoic oceans. *Earth and Planetary Science Letters*, 84 (1), 27–41. doi: 10.1016/0012-821X(87)90173-7
- Kobluk, D., and Lysenko, M. (1986). Reef-dwelling molluscs in open framework cavities, Bonaire N.A., and their potential for preservation in a fossil reef. *Bulletin of Marine Science*. 39, 657–672.
- Kumpan, T., Kalvoda, J., Bábek, O., Holá, M., and Kanický, V. (2019). Tracing paleoredox conditions across the Devonian–Carboniferous boundary event: A case study from carbonate-dominated settings of Belgium, the Czech Republic, and northern France. *Sedimentary Geology* 380, 143–157. doi: 10.1016/j.sedgeo.2018.12.003
- Lan, C., Xu, Z., Yang, D., Yang, W., Lu, C., Chen, H., et al. (2022). Stratigraphy and depositional evolution of the terminal Ediacaran platform in the central to northern Sichuan Basin, Southwest China. *Palaeogeography Palaeoclimatology Palaeoecol.* 601, 111142. doi: 10.1016/j.palaeo.2022.111142
- Léonide, P., Floquet, M., and Villier, L. (2007). Interaction of tectonics, eustasy, climate and carbonate production on the sedimentary evolution of an early/middle Jurassic extensional basin (Southern Provence Sub-basin, SE France). *Basin Res.* 19, 125–152. doi: 10.1111/j.1365-2117.2007.00316.x
- Li, G., Steiner, M., Zhu, X., Yang, A., Wang, H., and Erdtmann, B. D. (2007). Early Cambrian metazoan fossil record of South China: Generic diversity and radiation patterns. *Palaeogeography Palaeoclimatology Palaeoecol.* 254, 229–249. doi: 10.1016/j.palaeo.2007.03.017
- Li, X., Yu, M., Lehrmann, D. J., Payne, J. L., Kelley, B. M., and Minzoni, M. (2012). Factors controlling carbonate platform asymmetry: Preliminary results from the Great Bank of Guizhou, an isolated Permian–Triassic Platform in the Nanpanjiang Basin, south China. *Palaeogeography Palaeoclimatology Palaeoecol.* 315–316, 158–171. doi: 10.1016/j.palaeo.2011.11.023
- Liu, B., Xu, X., Luo, A., and Kang, C. (1987). Storm events and phosphate deposition in Cambrian on the western margin of the Yangtze Platform, China. *Acta Sedimentologica Sinica* 5(3), 28–39.
- Liu, H., Tan, X., Li, Y., Cao, J., and Luo, B. (2018). Occurrence and conceptual sedimentary model of Cambrian gypsum-bearing evaporites in the Sichuan Basin, SW China. *Geosci. Front.* 9, 1179–1191. doi: 10.1016/j.gsf.2017.06.006
- Lokier, S. W., Wilson, M. E. J., and Burton, L. M. (2009). Marine biota response to clastic sediment influx: A quantitative approach. *Palaeogeography Palaeoclimatology Palaeoecol.* 281, 25–42. doi: 10.1016/j.palaeo.2009.07.007
- Loreau, J.-P., and Purser, B. H. (1973). *Distribution and Ultrastructure of Holocene Ooids in the Persian Gulf* (Berlin, Heidelberg: Springer Berlin Heidelberg), 279–328.
- Lu, C., Hao, F., Zou, H., Koeshidayatullah, A., Manche, C. J., Li, P., et al. (2025). Testing the viability of normal seawater dolomitization in lower Cambrian carbonates using clumped isotopes. *Sedimentology*. 72, 713–733. doi: 10.1111/sed.13256
- Lu, C., Liu, Z., Jia, H., Tian, H., Zou, H., Dai, Q., et al. (2019). The eogenetic karst of the Cambrian Longwangmiao Formation in the Yangtze Platform: Implications for the eustatic and stratigraphic correlations of Toyonian (Cambrian). *Geological Journal*. 54, 3720–3736. doi: 10.1002/gj.v54.6
- Lu, C. J., Liu, Z., Tian, H. Q., Liu, M. J., Lin, J. H., Wang, Y., et al. (2018). An eogenetic paleokarst model controlled by multi-level sea-level: A case study of Shilongdong formation in Lower Cambrian, from the west Hubei and the east Chongqing to the west Hunan and Hubei, SW China. *Journal of China University of Mining & Technology*, 47 (5), 1167–1179.
- Ma, Y. S., Chen, H. D., and Wang, G. L. (2009). The tectonic-sequence lithofacies paleogeography in South China. Beijing: China Science Publishing & Media Ltd.
- Ma, Z. X., Li, B., and Liu, X. T. (2015). Geochemical Characteristics and Implications for the Evolution of Sedimentary Environments of Early Cambrian Qingxudong Formation in Eastern Guizhou, Southwestern China. *Geological Science and Technology Information*, 34 (2), 71–77
- McLennan, S. M. (1993). Weathering and global denudation. *J. Geology* 101, 295–303. doi: 10.1086/648222
- Mei, M., Zhang, H., Meng, X., and Chen, Y. (2006). Sequence stratigraphic division and framework of the Lower Cambrian in the Upper Yangtze region. *Geology In China* 33, 1292–1304. doi: 10.12029/gc20060612
- Mutti, M., and Hallock, P. (2003). Carbonate systems along nutrient and temperature gradients: some sedimentological and geochemical constraints. *Int. J. Earth Sci.* 92, 465–475. doi: 10.1007/s00531-003-0350-y
- Nesbitt, H. W. (1979). Mobility and fractionation of rare earth elements during weathering of a granodiorite. *Nature* 279, 206–210. doi: 10.1038/279206a0
- Nesbitt, H. W., and Young, G. M. (1982). Early Proterozoic climates and plate motions inferred from major element chemistry of lutites. *Nature* 299, 715–717. doi: 10.1038/299715a0
- Pfeil, R. W., and Read, J. F. (1980). Cambrian carbonate platform margin facies, Shady Dolomite, southwestern Virginia, U.S.A. *J. Sedimentary Res.* 50, 91–116. doi: 10.1306/212F7978-2B24-11D7-8648000102C1865D

- Pomar, L., and Haq, B. U. (2016). Decoding depositional sequences in carbonate systems: Concepts vs experience. *Global Planetary Change* 146, 190–225. doi: 10.1016/j.gloplacha.2016.10.001
- Purkis, S. J., Harris, P. M., and Lokier, S. (2017). Quantitative interrogation of a fossilized carbonate sand body - The Pleistocene Miami oolite of South Florida. *Sedimentology* 64, 1439–1464. doi: 10.1111/sed.2017.64.issue-5
- Read, J. F. (1985). Carbonate platform facies models. *AAPG Bull.* 69, 1–21. doi: 10.1306/AD461B79-16F7-11D7-8645000102C1865D
- Read, J., and Pfeil, R. (1983). Fabrics of allochthonous reefal blocks, Shady Dolomite (Lower to Middle Cambrian), Virginia Appalachians. *J. Sedimentary Res.* 53, 761–778. doi: 10.1306/AD461B79-16F7-11D7-8645000102C1865D
- Ren, Y., Zhong, D., Gao, C., Li, B., Cao, X., Wang, A., et al. (2019). The paleoenvironmental evolution of the Cambrian Longwangmiao Formation (Stage 4, Toyonian) on the Yangtze Platform, South China: Petrographic and geochemical constrains. *Mar. Petroleum Geology* 100, 391–411. doi: 10.1016/j.marpetgeo.2018.10.022
- Ren, Y., Zhong, D., Liu Liang, H. T., Sun, H., Gao, C., and Zheng, X. (2018). Isotopic and elemental evidence for paleoenvironmental evolution of Cambrian Stage 4 Longwangmiao Formation, east Chongqing, China. *Earth Science*, 2018, 43(11), 4066–4095.
- Ren, Y., Zhong, D., Gao, C., Liang, T., Sun, H., Wu, D., et al. (2017). High-resolution carbon isotope records and correlations of the lower Cambrian Longwangmiao formation (stage 4, Toyonian) in Chongqing, South China. *Palaeogeography Palaeoclimatology Palaeoecol.* 485, 572–592. doi: 10.1016/j.palaeo.2017.07.013
- Saltzman, M. R. (1999). Upper Cambrian carbonate platform evolution, Elvinia and Taenicephalus zones (pterocephaliid-ptychaspid bioterm boundary), northwestern Wyoming. *J. Sedimentary Res.* 69, 926–938. doi: 10.2110/jsr.69.926
- Sardar Abadi, M., Kulagina, E. L., Voeten, D. F. A. E., Boulvain, F., and Da Silva, A.-C. (2017). Sedimentologic and paleoclimatic reconstructions of carbonate factory evolution in the Alborz Basin (northern Iran) indicate a global response to Early Carboniferous (Tournaisian) glaciations. *Sedimentary Geology* 348, 19–36. doi: 10.1016/j.sedgeo.2016.11.011
- Schröder, S., Grotzinger, J. P., Amthor, J. E., and Matter, A. (2005). Carbonate deposition and hydrocarbon reservoir development at the Precambrian–Cambrian boundary: The Ara Group in South Oman. *Sedimentary Geology* 180, 1–28. doi: 10.1016/j.sedgeo.2005.07.002
- Shen, A., Chen, Y., Pan, L., Wang, L., and She, M. (2018). Facies and porosity origin of reservoirs: Case studies from the Cambrian Longwangmiao Formation of Sichuan Basin, China, and their implications on reservoir prediction. *J. Natural Gas Geosci.* 3, 37–49. doi: 10.1016/j.jnggs.2018.03.003
- Šimíček, D., Bábek, O., Faměra, M., and Kalvoda, J. (2020). Million-year secular variations in the elemental geochemistry of Devonian marine records and a link to global climate and bioevents: Prague Basin, Czechia. *Sedimentary Geology* 402, 105651. doi: 10.1016/j.sedgeo.2020.105651
- Smith, L. B. Jr., Eberli, G. P., and Sonnenfeld, M. (2004). “Sequence-stratigraphic and paleogeographic distribution of reservoir-quality dolomite, madison formation, wyoming and montana,” in *Integration of Outcrop and Modern Analogs in Reservoir Modeling*. Eds. G. M. Grammer, P. M. M. Harris and G. P. Eberli (American Association of Petroleum Geologists).
- Strasser, A. (1986). Ooids in Purbeck limestones (lowermost Cretaceous) of the Swiss and French Jura. *Sedimentology*, 33, 711–727. doi: 10.1111/j.1365-3091.1986.tb01971.x
- Tan, Q., Shi, Z. J., Tian, Y. M., Wang, Y., and Wang, C. C. (2017). Origin of ooids in ooidal-muddy laminites: A case study of the lower Cambrian Qingxudong Formation in the Sichuan Basin, South China. *Geological J.* 53, 1716–1727. doi: 10.1002/gj.2995
- Torsvik, T. H., and Cocks, L. R. M. (2013). Chapter 2 New global palaeogeographical reconstructions for the Early Palaeozoic and their generation. Geological Society, London, Memoirs, 38, 5–24.
- Tucker, M. E., and Wright, V. P. (1990). Carbonate depositional systems I: marine shallow-water and lacustrine carbonates. *Carbonate Sedimentology*, 101–227. doi: 10.1002/9781444314175
- Vail, P. R., Mitchum, R. M. Jr., and Thompson, S. III (1977). “Seismic stratigraphy and global changes of sea level, part 4: global cycles of relative changes of sea level,” in *Seismic Stratigraphy — Applications to Hydrocarbon Exploration*. Ed. C. E. Payton (American Association of Petroleum Geologists).
- Wang, H., and Zhou, J. (2000). Data Smoothing and Distortion of X-ray Diffraction Peaks. I. Theory. *Journal of Applied Crystallography - J APPL CRYST.* 33, 1128–1135. doi: 10.1107/S0021889800006932
- Woolfe, K. J., and Larcombe, P. (1999). Terrigenous sedimentation and coral reef growth: a conceptual framework. *Mar. Geology* 155, 331–345. doi: 10.1016/S0025-3227(98)00131-5
- Wyn, G., and Hughes, G. (2004). Middle to Upper Jurassic Saudi Arabian carbonate petroleum reservoirs: biostratigraphy, micropalaeontology and palaeoenvironments. *Geoarabia-Manama* 9, 79–114. doi: 10.2113/geoarabia090379
- Xie, L., Yang, X., Zhang, Y., Xu, Y., Zeng, D., Tang, R., et al. (2024). Sedimentary characteristics and lithofacies paleogeography of the Cambrian in Sichuan basin, Southwest China. *Petroleum* 10, 224–242. doi: 10.1016/j.petlm.2022.02.003
- Yang, J., Cawood, P. A., Du, Y., Li, W., and Yan, J. (2016). Reconstructing Early Permian tropical climates from chemical weathering indices. *Geological Soc. America Bull.* 128, 739–751. doi: 10.1130/B31371.1
- Yang, X., Wang, Y., and Wang, X. (2017). Evaluation of dolomite reservoirs in the Longwangmiao Formation, Lower Cambrian in Northern Sichuan basin, China[J]. *Petroleum*. (2017) 3(4), 406–413
- Zhang, P., Liu, G., Cai, C., Li, M., Chen, R., Gao, P., et al. (2019). Alteration of solid bitumen by hydrothermal heating and thermochemical sulfate reduction in the Ediacaran and Cambrian dolomite reservoirs in the Central Sichuan Basin, SW China. *Precambrian Res.* 321, 277–302. doi: 10.1016/j.precamres.2018.12.014
- Zhou, X., Li, J., Wang, H., and Li, W. (2014). Reconstruction of cambrian global paleo-plates and paleogeography. *Mar. Origin Petroleum Geology*. 19(02):1–7.
- Zhu, M.-Y., Babcock, L. E., and Peng, S.-C. (2006). Advances in Cambrian stratigraphy and paleontology: Integrating correlation techniques, paleobiology, taphonomy and paleoenvironmental reconstruction. *Palaeoworld* 15, 217–222. doi: 10.1016/j.palwor.2006.10.016
- Zuo, J., Peng, S., Qi, Y., Zhu, X., Bagnoli, G., and Fang, H. (2018). Carbon-isotope excursions recorded in the cambrian system, south China: implications for mass extinctions and sea-level fluctuations. *J. Earth Sci.* 29, 479–491. doi: 10.1007/s12583-017-0963-x